

Photogrammetric Image Registration (PIR) of MTI Imagery

P. Pope and J. Theiler*

Space and Remote Sensing Sciences Group
Los Alamos National Laboratory, Los Alamos, NM

ABSTRACT

This paper describes the use of photogrammetric principles to georeference imagery collected by the Multispectral Thermal Imager (MTI) satellite. The photogrammetric image registration (PIR) method consists of two main parts. The first part estimates a trajectory (exterior orientation as a function of time) for the sensor based on a photogrammetric bundle adjustment governed by user defined ground control points. The ground control points are defined by manual identification of conjugate points between the LEVEL1B_U imagery and reference data (an orthoimage and a digital elevation model derived from aerial photography). The second part uses this trajectory as input to a direct georeferencing method to determine the location of each pixel in the imagery. The PIR method uses mathematical models of the sensor, its trajectory, timing, and the terrain to mimic the actual image acquisition event. It was found that accurate calculation of the exterior orientation parameters was not a requirement to obtain accurately georeferenced imagery. This is particularly intriguing, and deserves more in-depth study, because the values of the exterior orientation parameters solved for through photogrammetric bundle adjustment are known to be in disagreement with the actual motion of the satellite platform. The individual steps of the PIR method, the mathematical models used, and the results of georeferencing MTI imagery through the use of this approach are described.

Keywords: MTI, registration, photogrammetry, collinearity, bundle adjustment, direct georeferencing

The fifteen-channel Multispectral Thermal Imager (MTI) provides accurately calibrated satellite imagery for a variety of scientific and programmatic purposes. Imagery is collected by sixteen linear CCD arrays (one for each band, with bands H1 and H2 being redundant) arranged on three sensor chip assemblies (SCAs) (Fig. 1). Individual arrays are turned on in a timing sequence that is designed to maximize the overlap of the ground coverage for all of the bands. Although viewing geometries encountered under operational conditions vary substantially from one image to another (especially for the off-nadir images), the same timing sequence is used for each image acquisition. This leads to varying band-to-band alignments within an SCA, and between the different SCAs, of the imagery contained in the LEVEL1B_U product. To be useful for spectral analysis and physical retrievals, such as water surface temperature and land cover classification, the calibrated pixels from the individual detectors on the focal plane of this pushbroom sensor must be resampled to a regular grid corresponding to the observed scene on the ground¹. Therefore, the registration of MTI imagery requires methods to address the band-to-band and SCA-to-SCA misregistrations present in the LEVEL1B_U imagery. Compensating for these effects permits a single image stack of all sixteen bands from all three SCAs to be created. We have developed several image registration algorithms to meet this need².

This paper describes an image registration approach which is based on photogrammetric principles. The main idea of the photogrammetric image registration (PIR) method is to recreate the image acquisition event with enough fidelity such that an accurately georeferenced image can be produced through direct georeferencing. This method is similar to our standard approach, which also uses a direct georeferencing approach³. The main difference between this approach and our standard approach is the source of the trajectory information. In our standard approach, the trajectory information is measured by a Global Positioning System (GPS) receiver and an Inertial Measurement Unit (IMU) on-board the satellite platform. The data collected by these instruments are telemetered from the satellite to the ground station. In the PIR approach, the trajectory information is derived through the use of a photogrammetric bundle adjustment.

*papope@lanl.gov, jt@lanl.gov

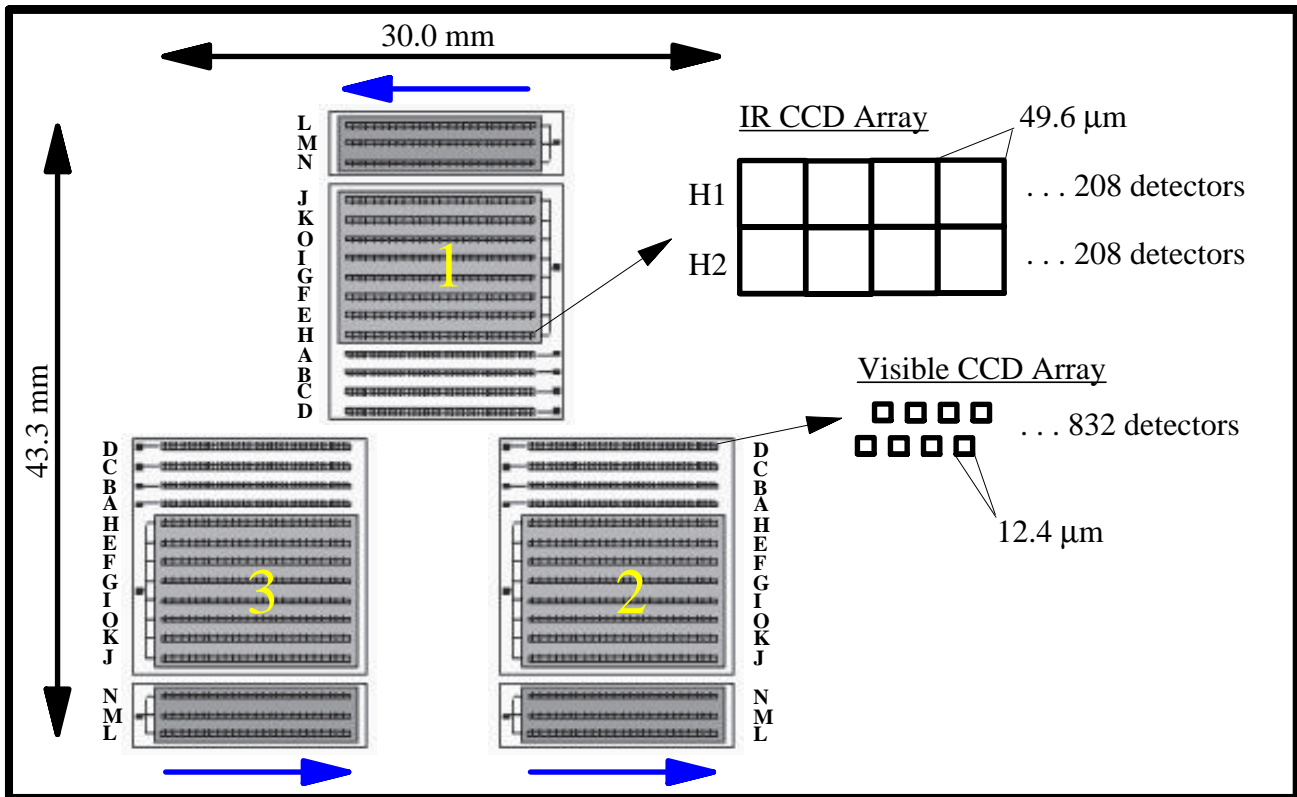


Figure 1. Illustration of the MTI focal plane layout. The SCA numbers are in yellow, and the blue arrows indicate the readout directions.

Other differences between our standard approach and the PIR method are the coordinate systems, the projection surface, and the alignment of the output grid used to create the final image product. Our standard approach models the relative motions of the Earth and the MTI satellite, and uses a flat plane as the projection surface, while the PIR method uses a static, cartographic coordinate system, and projects the imagery onto a model of the terrain surface. Therefore, our standard method produces rectified imagery, while the PIR method produces orthorectified imagery. Our standard approach produces imagery which is registered to either an orbit-aligned or a geo-aligned output grid, whereas the PIR method only outputs imagery registered to a geo-aligned output grid. Also, our standard approach is primarily an autonomous method, whereas the PIR method requires manually derived user input.

In our operational experience, there have been MTI acquisitions for which the trajectory information was unavailable. This was the primary motivation to research and develop a photogrammetric-based method which could register MTI imagery in those instances when the measured trajectory information was unavailable. It supports and complements our standard approach.

2. METHODOLOGY

The PIR method approaches the problem of georeferencing MTI imagery in two main parts. The first part estimates a trajectory for the sensor through the use of a photogrammetric bundle adjustment. The second part uses this derived trajectory to georeference the imagery through the use of the direct georeferencing method. Each of these steps utilize mathematical models to mimic the image acquisition process. These models are described first. Then the two main steps of the PIR method are explained.

2.1 Models

The PIR method makes use of various models to simulate the image acquisition event. The models used are a sensor model, a trajectory model, a timing model, and a terrain model. The PIR method also makes use of two spatial coordinate systems; a sensor coordinate system and a geo coordinate system. The sensor coordinate system and geo coordinate system are sometimes referred to in the remote sensing literature as the "image-space" and "object-space", respectively. Each of these models and coordinate systems are described next.

2.1.1. Sensor Model

The sensor model is defined within the sensor coordinate system (Fig. 2). The x-axis points in the direction of flight, the y-axis points in the port direction, and the z-axis points away from nadir. The origin of the sensor coordinate system is located at the focal point of the sensor model. The individual detectors of the MTI pushbroom sensor model are located on a flat plane, positioned a distance equal to the focal length below the origin of the sensor coordinate system. The focal length of the MTI sensor is approximately 1.251 meters. The sensor model also defines the location of each detector on the focal plane, the three components (cosine angles) of the unit length line-of-sight (LOS) ray associated with each detector on the focal plane, and the location of the focal point. Since this information is constant, it is calculated once and stored in a database. The values for these quantities were calculated from pre-flight geometric calibration work^{4,5}. Although this sensor model is a simplification of the actual MTI sensor geometry, we have found it to be useful.

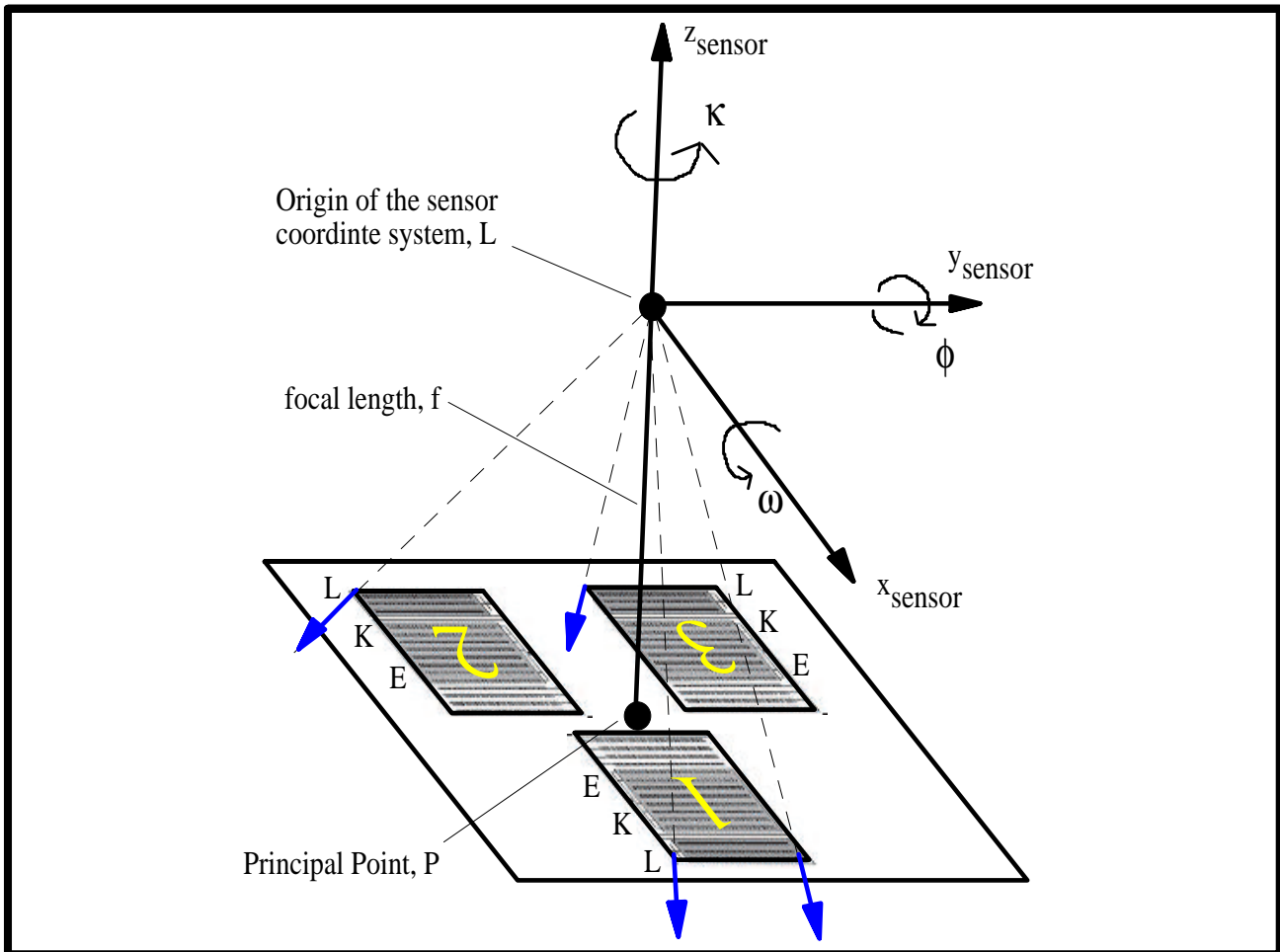


Figure 2. Illustration of the sensor model. The focal length "f" lies between the origin of the sensor coordinate system "L" and the principal point "P". The direction of positive attitude angles (i.e. "right hand rule") are indicated. The yellow numbers mark the position of the three SCAs. For clarity, only the bands used in this research are shown. A few LOS rays (blue arrows) are shown.

2.1.2 Trajectory Model

The trajectory of the sensor model, as described within the geo coordinate system, is modeled by using six exterior orientation parameters; three for position and three for attitude. Each of the exterior orientation parameters is modeled as a second order polynomial in time,

$$q = q_0 + q_1t + q_2t^2 \quad (1)$$

where t is the scan time, and q corresponds to ω , ϕ , κ , X_L , Y_L , or Z_L (Fig. 2). A scan time of zero is defined as the instant that the first scan line is acquired, typically by band L on SCA 1. Therefore, the timing scheme used in the PIR method is relative rather than absolute.

Note that Eq. (1) implies that there are three coefficients for each of the six exterior orientation parameters. Therefore, a total of eighteen coefficients are required to characterize the behavior of all six of the exterior orientation parameters with time. Note also that if the q_2 coefficient (i.e. acceleration) is set to zero, then the exterior orientation parameter is modeled as linear motion. And that if both the q_2 and q_1 coefficients (i.e. acceleration and velocity, respectively) are set to zero, then the exterior orientation parameter is modeled as a constant.

2.1.3 Timing Model

The timing model associates a single scan time with each scan line of the image acquired from a particular band and SCA of the sensor model. The scan time is given by,

$$t = s(i-1) + t_0 \text{ for } 1 \leq i \leq m \quad (2)$$

where s is the scan rate, i is the scan line number (image row number), t_0 is the time of first scan for the particular band and SCA being referenced, and m is equal to the number of scan lines (rows) in the image. The same (nominal) timing sequence (i.e. t_0 values) and scan rates are typically used for every MTI image acquisition, since it would be difficult from an operational standpoint to upload a timing sequence specifically designed for the roll and pitch of a particular overpass (Fig. 3). The scan rate for the "visible" bands (bands A, B, C, and D) is 0.000715546 seconds per scan line, while the scan rate for the "IR" bands (bands E through L) is 0.00286390 seconds per scan line. Note that the "IR" band scan rate is four times slower than the "visible" band scan rate, since an "IR" band detector element is four times as large as a "visible" band detector element (Fig. 1).

2.1.4 Terrain Model

The terrain model used by the PIR process is a raster of heights above a vertical datum. This type of data set is typically called a Digital Elevation Model (DEM). Prior to using the DEM within the PIR method, it must be georeferenced to the geo coordinate system, and the heights must be converted to heights above the x-y plane of the geo coordinate system.

2.2 The PIR Process

As mentioned previously, the PIR method approaches the problem of georeferencing MTI imagery in two main parts. The first part estimates a trajectory for the sensor through the use of a photogrammetric bundle adjustment. The second part uses this trajectory to georeference the spectrally calibrated imagery contained in the LEVEL1B_U product through the use of direct georeferencing. The use of the various models described previously in these two main parts is explained next.

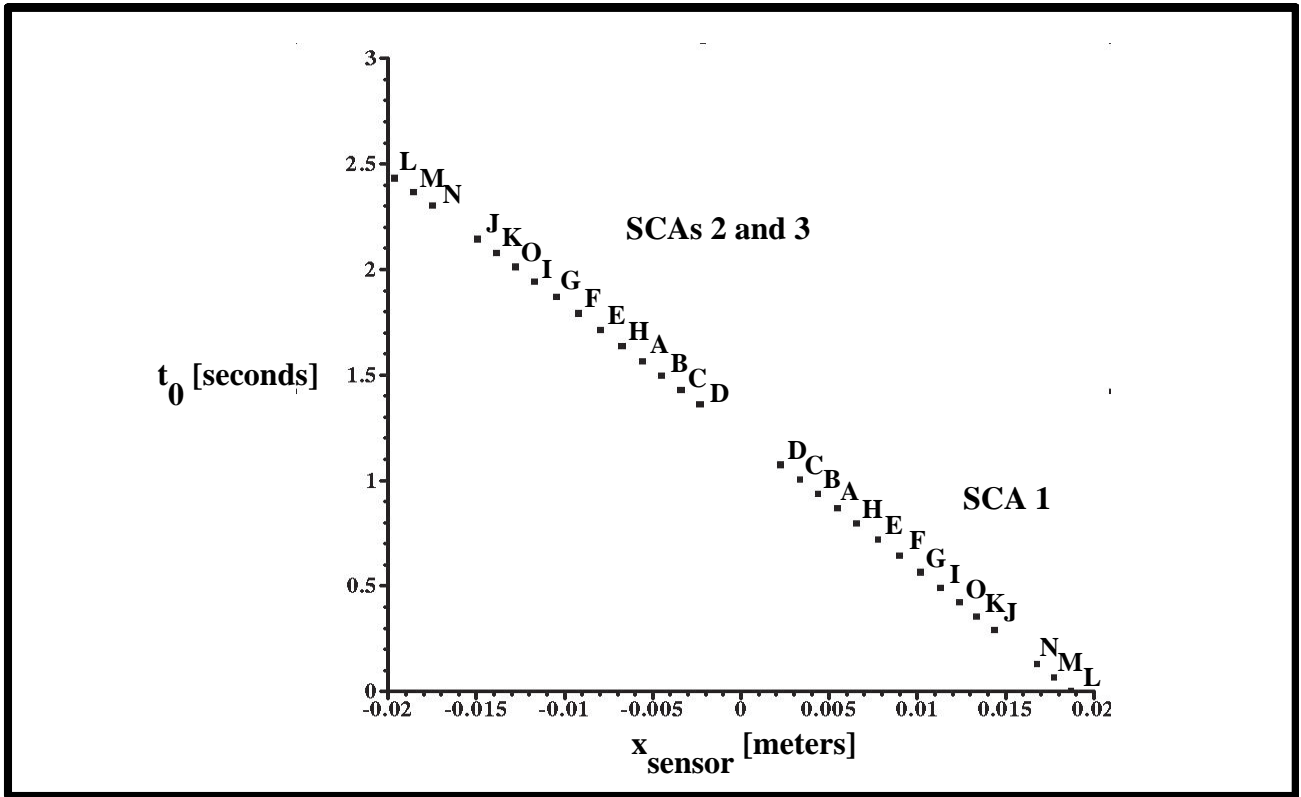


Figure 3. A plot of the nominal t_0 values for each band of each SCA.

2.2.1 Photogrammetric Bundle Adjustment

The PIR method uses a photogrammetric bundle adjustment to calculate the coefficients which govern the six exterior orientation parameters (Eq. 1). Photogrammetric bundle adjustment is a commonly used method for calculating the exterior orientation of a remote sensing instrument. Only a brief description is provided here. More details can be found in several references on this subject^{6,7,8}.

Photogrammetric bundle adjustment uses the numerical method of least squares to fit (i.e. regress) observation equations to predefined observations. The observation equations used are typically the collinearity equations,

$$x_a = -f \frac{m_{11}(X_A - X_L) + m_{12}(Y_A - Y_L) + m_{13}(Z_A - Z_L)}{m_{31}(X_A - X_L) + m_{32}(Y_A - Y_L) + m_{33}(Z_A - Z_L)} \quad (3)$$

and

$$y_a = -f \frac{m_{21}(X_A - X_L) + m_{22}(Y_A - Y_L) + m_{23}(Z_A - Z_L)}{m_{31}(X_A - X_L) + m_{32}(Y_A - Y_L) + m_{33}(Z_A - Z_L)} \quad (4)$$

where $(x_a, y_a, -f)$ is the location of a pixel on the focal plane of the sensor model, (X_L, Y_L, Z_L) is the location of the origin of the sensor coordinate system, (X_A, Y_A, Z_A) is the location of a feature on the ground, f is the focal length of the sensor model, and the m_{ij} are the elements of a rotation matrix governed by the three attitude parameters.

The collinearity equations express the fact that the location of a feature lying on the terrain surface (expressed within the geo coordinate system), the location of the image of that feature on the focal plane of the sensor model (expressed within the sensor coordinate system), and the focal point of the sensor model (expressed within the geo coordinate system) are all colinear (Fig. 4).

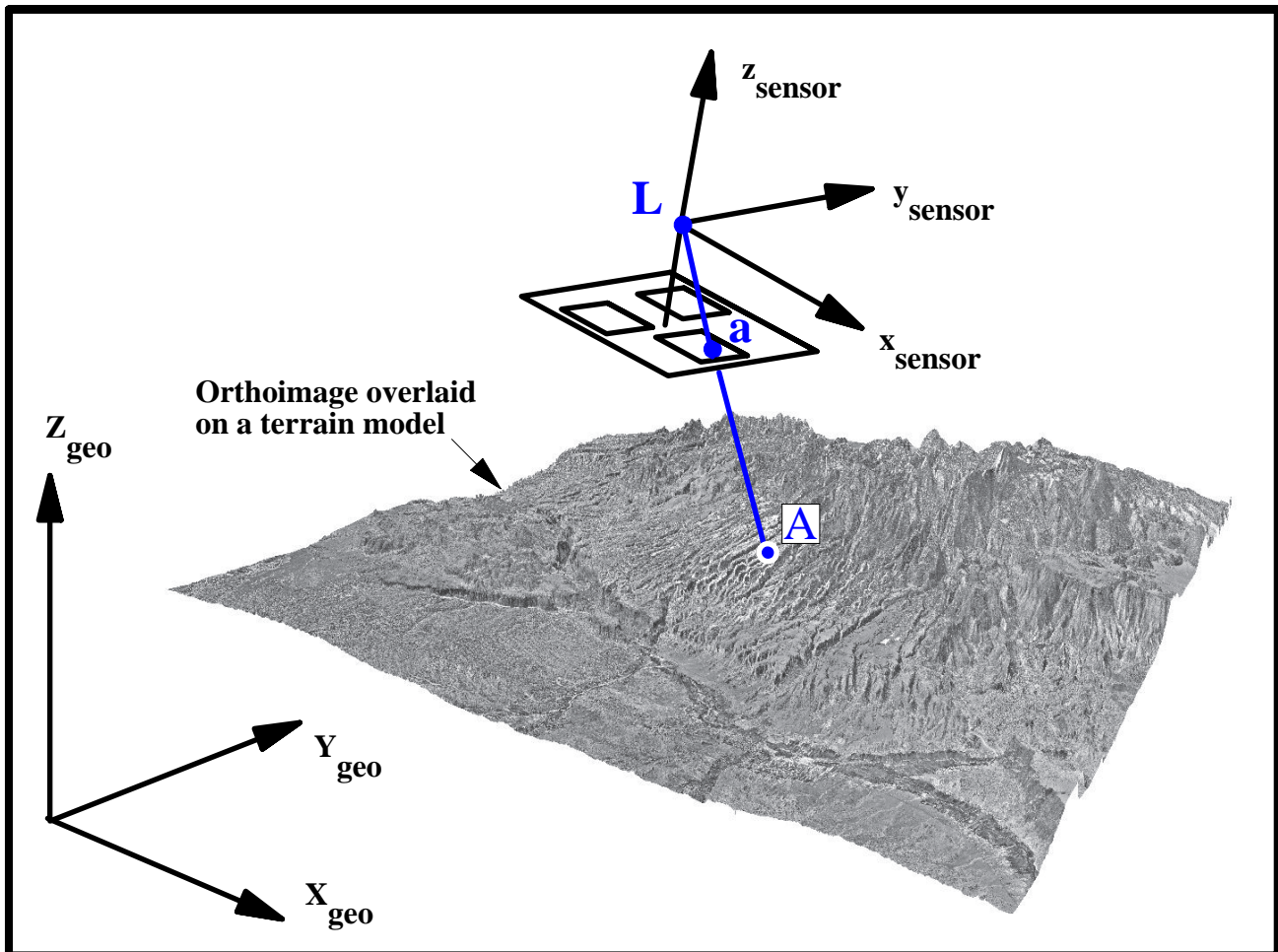


Figure 4. Illustration of the collinearity condition. The feature located at point "A" on the ground, the image of the feature located at point "a" on the focal plane, and the origin of the sensor coordinate system (i.e. the focal point) at "L", are collinear. The sensor model and the terrain model are not shown to scale.

The observations consist of multiple conjugate point pairs, usually called ground control points (GCPs). Each conjugate point pair is formed by associating image location of a feature (and thereby its location on the focal plane of the sensor model) with its actual location on the terrain surface (expressed within the geo coordinate system). For static imaging systems, such as an aerial mapping camera, the six exterior orientation parameters are constants associated with a single photograph. For dynamic imaging systems, such as whiskbroom and pushbroom sensors, the six exterior orientation parameters are functions of time.

The collinearity equations were modified such that the six exterior orientation elements were modeled as second order polynomial functions of time (Eq. 1). As is typically done to facilitate solution of the non-linear collinearity equations, the collinearity equations were linearized via a Taylor series expansion. Therefore, the least squares adjustment does not solve for the coefficients directly, rather it solves for corrections to initial approximations of the coefficients.

A photogrammetric bundle adjustment code was written in the Interactive Data Language (IDL)⁹ to solve for the second order polynomial coefficients for each of the six exterior orientation parameters. A capability to turn the solution of each coefficient "on" or "off" was also coded. This code takes a list of GCP observations as input, and outputs the solution to the coefficients. The residual errors in the x and y directions, as projected onto the focal plane of the sensor model, are also output.

2.2.2 Direct Georeferencing

After the trajectory model has been fully characterized by solving for the coefficients, each pixel can then be assigned a location in the geo coordinate system by using the direct georeferencing method. Direct georeferencing is a method which uses trajectory information (either gathered by direct measurements of the platform's motion, or estimated through photogrammetric methods, or a combination of the two) to georeference each pixel in the imagery by modeling the image acquisition event¹⁰. The sensor model is "flown" through the geo coordinate system by using the trajectory information, and "ray tracing" is used to intersect each LOS ray with the terrain model¹¹, thereby yielding a geolocation for the digital number of every pixel in the LEVEL1B_U image. This creates a three-dimensional dataset, sometimes referred to as a "point cloud", or a "point database". Therefore, each record in the point database consists of four fields; a digital number (e.g. calibrated radiance), and its X, Y, and Z location within the geo coordinate system. Ancillary information can also be calculated during ray tracing and included as additional fields in the point cloud database. For example, the slope and aspect at each pixel's geolocation could be calculated from the DEM. This information would facilitate analysis of the directional reflectance properties of the land cover.

To be useful for image processing analysis, each point database created by the direct georeferencing process must be converted to a raster format. The PIR method creates a georeferenced image from each point database by first creating a triangulated irregular network (TIN). Bilinear interpolation is used to resample the irregularly spaced digital numbers onto a regular grid. The ground sample distance (GSD) and extents of the regular grid are set by the user. This can be performed for the point database associated with each band from each SCA in a separate fashion, or the three point databases for any particular band from each SCA can be easily mosaicked by simply concatenating the point databases before creating the TIN. Since the direct georeferencing process inherently models the spatial distortions due to terrain relief, the georeferenced raster produced by this post-processing step is an orthoimage.

3. APPLICATION

The following sections describe use of the PIR method to georeference an MTI image. Although this single example is not a rigorous test of this method, it does serve to illustrate the processing steps. Actual versus estimated exterior orientation parameter values are compared, and a planimetric accuracy assessment of the georeferenced imagery produced by the PIR method are described. It also provides evidence that an accurately georeferenced image can be obtained even if the trajectory of the sensor model does not agree with the "true" viewing geometry during the actual image acquisition event.

The polynomial coefficients for two trajectory models were calculated through photogrammetric bundle adjustment. The first trajectory model assumed that all six of the exterior orientation parameters could be modeled as second order polynomials in time. Therefore, the solution for eighteen coefficients was required. This scenario was called the "full trajectory model". The second trajectory model assumed that the horizontal motion could be described as linear functions in time, and that the height was constant. In addition, the attitude of the sensor model was assumed to be constant, with κ fixed at a value close to 90 degrees (i.e. the sensor was moving from the South to the North), and the ω and ϕ angles set to zero. Therefore, the solution to six coefficients was required for this second scenario. This scenario was called the "reduced trajectory model".

3.1 MTI Image

The MTI image used was acquired on November 20, 2001 over Los Alamos, New Mexico (Table 1). Position and attitude information, as measured by the GPS receiver and IMU on-board the MTI satellite, were available for this acquisition (Table 2).

Table 1. General characteristics of the MTI image.

Image ID	107766
Image Start Time (UTC)	18:02:44.499
Image Stop Time (UTC)	18:02:50.506
Image Acquisition Time Interval	6.007 seconds
Number of Visible Scan Lines Acquired	4993
Number of IR Scan Lines Acquired	1249
Target Latitude	+35.8750 degrees
Target Longitude	-106.324 degrees
Target Elevation	1.999 kilometers (above the WGS84 datum)

Table 2. Exterior orientation characteristics of the MTI image.

Exterior Orientation Parameter	Measured Value
Latitude	+35.9332 degrees
Longitude	-106.504 degrees
Altitude	580.206 kilometers (above the WGS84 datum)
Roll	1.981 degrees
Pitch	-1.391 degrees
Pitch Rate	0.0277 degrees / second
Yaw	-0.669 degrees
Velocity	7,571 meters / second
Heading	99.102 degrees

3.2 Reference Data

The reference data consisted of an orthoimage and a DEM (Fig. 5). The source for these reference data were products created from aerial photography by the U.S. Geological Survey (USGS). The reference orthoimage was created by mosaicking sixtyfour, 1 meter resolution USGS Digital Orthoimage Quarter Quads (DOQQs). The reference DEM was created by mosaicking sixteen, 10 meter resolution USGS DEMs. A geospatial analysis software program called TNT MIPS¹² was used to create the reference orthoimage and DEM from the USGS products. The orthoimage was used to define GCPs, and the DEM served as the terrain model. The DEM data were converted from elevations above the National Geodetic Vertical Datum of 1929 (NGVD29) in meters, to heights above the World Geodetic System datum of 1984 (WGS84) in meters. This was achieved by subtracting the geoid separation distance (i.e. 18 meters) from each cell value. Both data sets were georeferenced to the Universal Transverse Mercator (UTM) coordinate system, Zone 13 North (based on the WGS84 datum) in units of meters. Therefore, the geo coordinate system used was a cartesian coordinate system whose horizontal (planimetric) and vertical (height) axes were based on the WGS84 datum. The X_{geo} axis was the UTM Easting axis, the Y_{geo} axis was the UTM Northing axis, and the Z_{geo} axis was associated with height above the WGS84 datum.

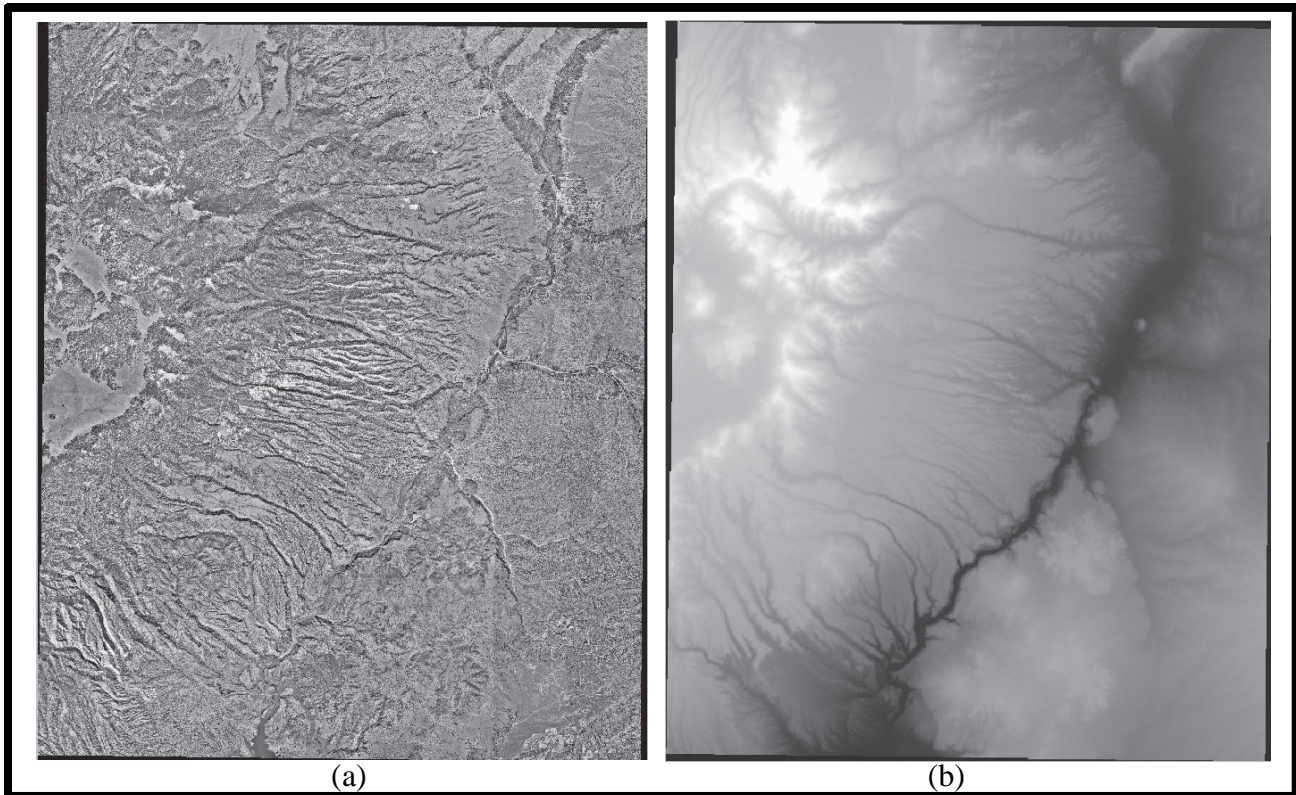


Figure 5. The reference orthoimage (a) and DEM (b). Both rasters are georeferenced to UTM Zone 13 North, based on the WGS84 datum. The darker and lighter features in the DEM are lower and higher elevations, respectively. The heights in the DEM span the range 1,602 meters to 3,522 meters above the WGS84 datum. Los Alamos, New Mexico is located at the center of each raster.

3.3 Ground Control Points

The LEVEL1B_U band L images associated with each SCA were used to define GCPs. Band L was chosen since the CCD arrays for this band are located farthest from the principal point than any other band (Fig. 2). Also, one GCP was placed near each corner of the three band L images. Defining GCPs in this manner was expected to yield the most accurate solution from the photogrammetric bundle adjustment, since these observations spanned the largest range for the input variables (i.e. time, x_a , y_a , X_A , Y_A , and Z_A).

Eight GCPs were manually defined for each image. Therefore, there were a total of 24 GCPs used as observations in each of the two photogrammetric bundle adjustments. Since each GCP is associated with a pair of equations (Eq.s (3) and (4)), these 24 GCPs permitted a system of 48 observation equations to be defined. These GCPs were created by displaying an MTI image next to the reference image and manually selecting conjugate point pairs (Fig. 6). The GCP tool in the Environment for Visualizing Imagery (ENVI)¹³ software program was used to perform this task. Once the image location of a GCP had been selected, the location within the sensor coordinate system (x_a, y_a) could be obtained by using the focal plane database, and the time of acquisition of each pixel could be calculated by using Eq. (2). Since the reference image was georeferenced, the horizontal position of each point within the geo coordinate system (X_A, Y_A) could be found, and its vertical position (Z_A) could be set by selecting the cell value from the DEM at that geolocation (Table 3).

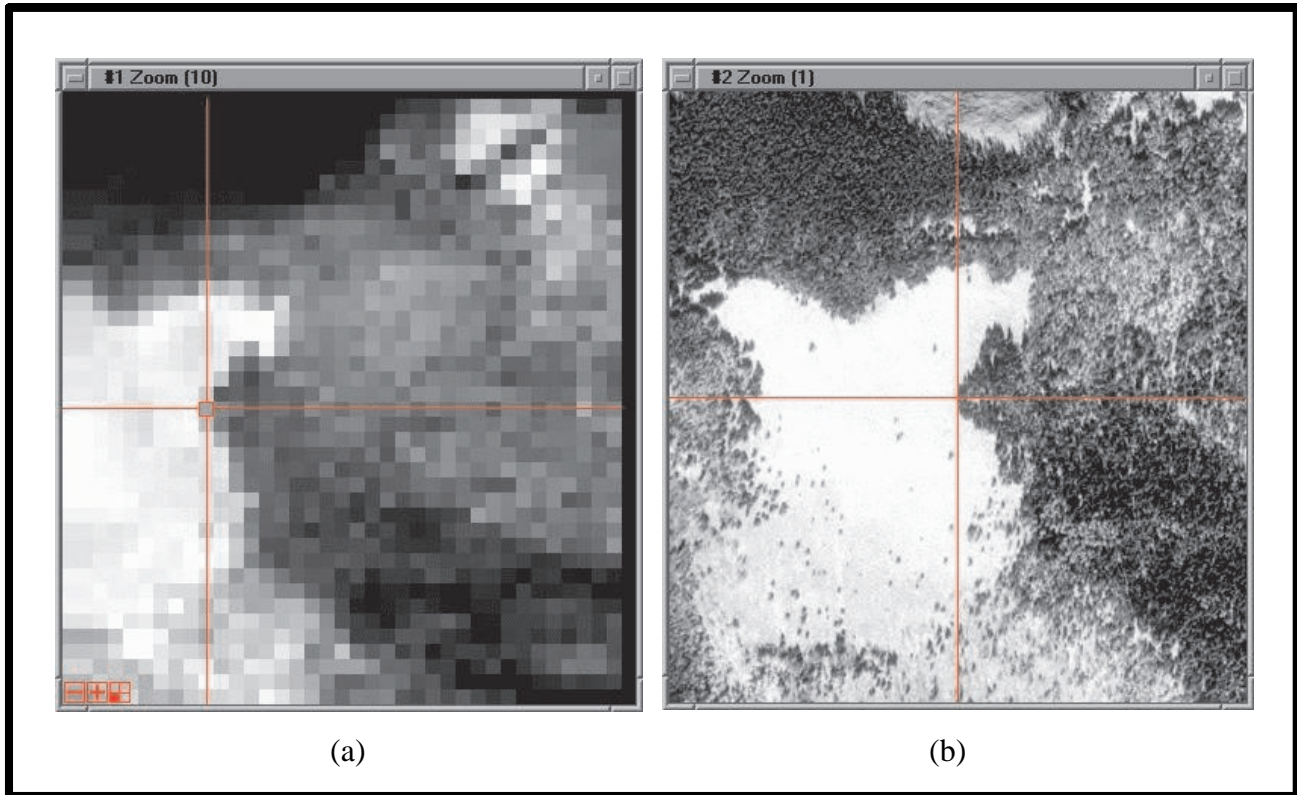


Figure 6. Example of setting a GCP through conjugate point definition. The image of a point on a forest edge as it appears in the LEVEL1B_U band L image from SCA 1 (a) is matched with the same feature as it appears in the reference orthoimage (b).

Table 3. The observations associated with the GCP of Figure 6.

Time [s]	x_a [m]	y_a [m]	X_A [m]	Y_A [m]	Z_A [m]
2.23710682	0.01876405	0.00476544	376,960.0	3,979,222.0	3,123.0

3.4 Full Trajectory Model

The IDL photogrammetric bundle adjustment code was used to solve for the 18 coefficients of the full trajectory model by using the 24 GCPs as input (Table 4). The residuals from the photogrammetric bundle adjustment were 1.4 pixels in the x_{sensor} direction and 1.3 pixels in the y_{sensor} direction. The total RMSE was 2.0 pixels.

Table 4. The coefficient values solved for by photogrammetric bundle adjustment for the full trajectory model.

Parameter	X Position	Y Position	Z Position	Omega Attitude	Phi Attitude	Kappa Attitude
Position	$X_{L0} = 380,007$ [m]	$Y_{L0} = 3,975,335$ [m]	$Z_{L0} = 583,489$ [m]	$\omega_0 = -2.056$ [deg]	$\phi_0 = -0.286$ [deg]	$\kappa_0 = 98.631$ [deg]
Velocity	$X_{L1} = -1,100$ [m/s]	$Y_{L1} = -618$ [m/s]	$Z_{L1} = -610$ [m/s]	$\omega_1 = 0.665$ [deg/s]	$\phi_1 = 0.008$ [deg/s]	$\kappa_1 = -0.533$ [deg/s]
Acceleration	$X_{L2} = 1,018$ [m/s ²]	$Y_{L2} = 2,151$ [m/s ²]	$Z_{L2} = -15$ [m/s ²]	$\omega_2 = -0.213$ [deg/s ²]	$\phi_2 = 0.099$ [deg/s ²]	$\kappa_2 = 0.078$ [deg/s ²]

3.5 Reduced Trajectory Model

The IDL photogrammetric bundle adjustment code was used to solve for the 6 coefficients of the reduced trajectory model by using the 24 GCPs as input (Table 5). The residuals from the photogrammetric bundle adjustment, as projected onto the focal plane, were 1.6 pixels in the x_{sensor} direction and 1.5 pixels in the y_{sensor} direction. The total RMSE was 2.2 pixels.

Table 5. The coefficient values solved for by photogrammetric bundle adjustment for the reduced trajectory model. A * indicates coefficients whose solution was turned "off" in the IDL photogrammetric bundle adjustment code.

Parameter	X Position	Y Position	Z Position	Omega Attitude	Phi Attitude	Kappa Attitude
Position	$X_{L0} = 382,759$ [m]	$Y_{L0} = 3,954,460$ [m]	$Z_{L0} = 582,458$ [m]	$*\omega_0 = 0$ [deg]	$*\phi_0 = 0$ [deg]	$\kappa_0 = 97.717$ [deg]
Velocity	$X_{L1} = -1,075$ [m/s]	$Y_{L1} = 7,363$ [m/s]	$*Z_{L1} = 0$ [m/s]	$*\omega_1 = 0$ [deg/s]	$*\phi_1 = 0$ [deg/s]	$*\kappa_1 = 0$ [deg/s]
Acceleration	$*X_{L2} = 0$ [m/s ²]	$*Y_{L2} = 0$ [m/s ²]	$*Z_{L2} = 0$ [m/s ²]	$*\omega_2 = 0$ [deg/s ²]	$*\phi_2 = 0$ [deg/s ²]	$*\kappa_2 = 0$ [deg/s ²]

3.6 Post-processing

The full and reduced trajectory models were used as inputs to the direct georeferencing method to register the LEVEL1B_U imagery. The outputs were two georeferenced image stacks; one created by using the full trajectory model, and another created by using the reduced trajectory model (Fig. 7). The previously described method for mosaicking the imagery from all three SCAs for each band by simply concatenating the point database files was successfully used. Each image stack contained 16 bands with a GSD of 20 meters and covered an areal extent of approximately 29 kilometers (North to South) by 17 kilometers (East to West).

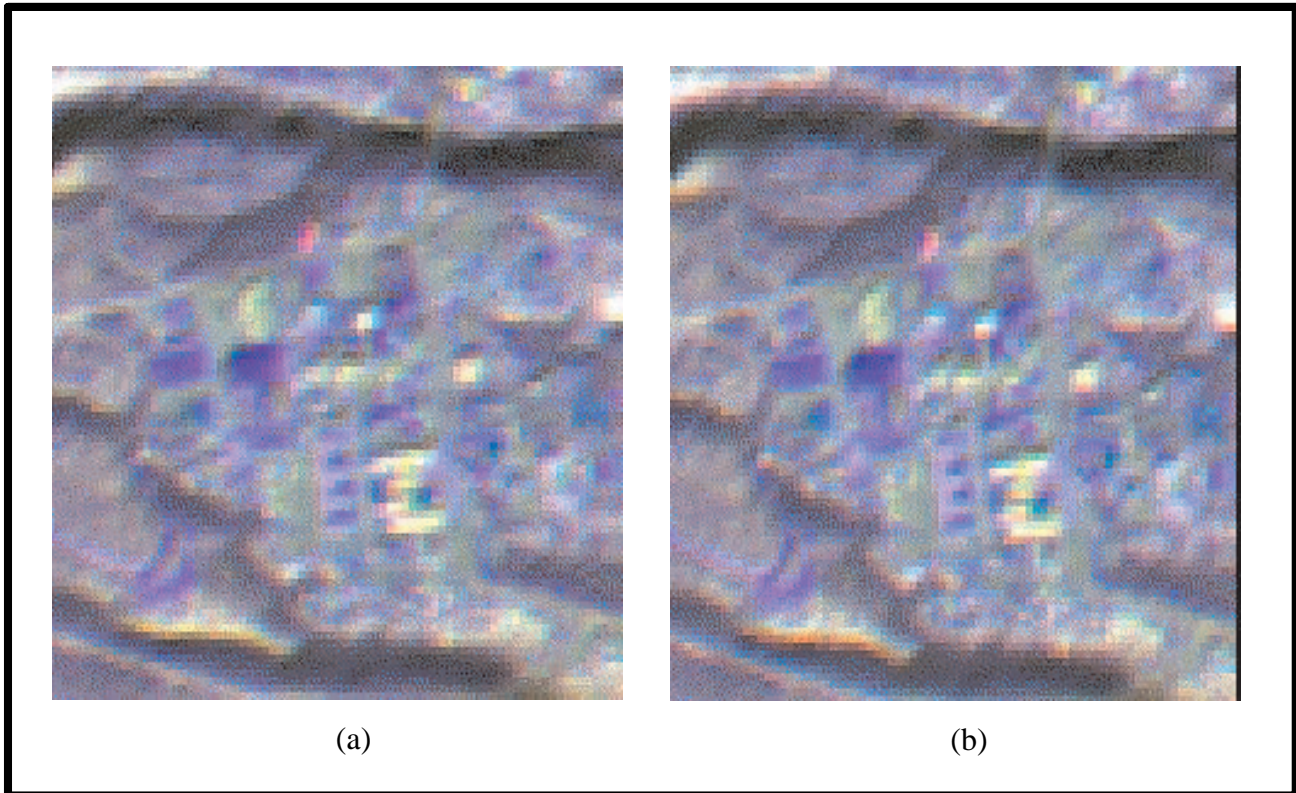


Figure 7. Subsections of the georeferenced imagery (bands L,K,E (RGB)) produced by the PIR method using the full (a) and the reduced (b) trajectory models. These subsections are of the main technical area (TA-03) at the Los Alamos National Laboratory.

3.7 Trajectory Comparison

The exterior orientation parameters associated with the measured trajectory of the MTI satellite and as derived from the full and reduced trajectory models were compared. Only a brief analysis was undertaken since the focus of this research was the planimetric accuracy of the georeferenced imagery produced by the PIR method. To facilitate the trajectory comparison, the values from Table 2 were converted to their approximate values as expressed in the sensor and geo coordinate systems used by the PIR method (Table 6).

Table 6. Converted exterior orientation characteristics of the MTI image.

Exterior Orientation Parameter	Measured Value
X_L	364,329 meters
Y_L	3,977,575 meters
Z_L	580,206 meters (above the WGS84 datum)
ω_0	-1.981 degrees
ϕ_0	1.391 degrees
ϕ_1	-0.0277 degrees / second
κ_0	97.633 degrees
Velocity	7,571 meters / second
Heading	99.102 degrees

In general, the full trajectory model (Table 4) is mostly inconsistent with the motions of the MTI satellite during image acquisition, while the reduced trajectory model (Table 5) is very similar. In particular, the accelerations of the full trajectory model are quite high, and the initial velocity of 1,402 meters per second is much slower than the actual velocity of 7,571 meters per second. Also, concerning the attitude of the sensor, only the initial roll (ω_0) and yaw (κ_0) of the full trajectory model are close to their actual values. The known pitch motion of the sensor has not been accurately captured by the full trajectory model. In contrast, the velocity (7,441 meters per second) and yaw (97.717 degrees) of the reduced trajectory model are close to their actual values. The flying height of the sensor (Z_{L0}) was captured by both trajectory scenarios.

3.8 Planimetric Accuracy Assessment

The georeferenced images for bands E, K, and L were compared with the reference orthoimage at 9 different locations. These bands were chosen since they include band L (the band used to define the GCPs), as well as the IR band farthest away from band L (band E, excluding band H), and the IR band located midway between these bands (band K). Accuracy assessment of these bands was assumed to be adequate to predict the planimetric accuracy of the other IR bands. At each location, the position of a well-defined feature was measured on both the reference orthoimage and the georeferenced image, and the difference in positions was calculated. This information was used to calculate summary statistics (Table 7 and Table 8).

Table 7. Location accuracy (mean and standard error) of the MTI imagery georeferenced by using the full trajectory model.

	Band L	Band K	Band E
Northing (Y_{geo})	0.5 ± 1.1 pixels	0.8 ± 0.8 pixels	1.2 ± 1.0 pixels
Easting (X_{geo})	1.5 ± 1.2 pixels	1.6 ± 0.9 pixels	1.7 ± 0.7 pixels
Overall	3.9 ± 1.0 pixels	3.4 ± 0.7 pixels	3.8 ± 0.6 pixels

Table 8. Location accuracy (mean and standard error) of the MTI imagery georeferenced by using the reduced trajectory model.

	Band L	Band K	Band E
Northing (Y_{geo})	2.5 ± 1.1 pixels	2.1 ± 0.8 pixels	1.7 ± 0.9 pixels
Easting (X_{geo})	-0.6 ± 0.6 pixels	-0.2 ± 0.5 pixels	-0.0 ± 0.2 pixels
Overall	3.4 ± 0.9 pixels	2.7 ± 0.8 pixels	2.6 ± 0.6 pixels

The planimetric accuracy in the Northing direction is higher for the full trajectory model imagery than it is for the reduced trajectory model imagery. The opposite is true in the Easting direction. Planimetric accuracy in both directions are lower for bands closer to the principal point for the reduced trajectory model imagery. The opposite is true for the full trajectory model imagery. The overall planimetric accuracy is higher for the reduced trajectory model imagery than it is for the full trajectory model imagery. Since the accuracy is of approximately the same magnitude (within one pixel) and orientation (positive or negative) for any particular direction (Northing or Easting), then the band-to-band registration is subpixel on average for both scenarios (Fig. 7). Combining the data from all three bands (i.e. 27 samples) for each scenario yielded an overall accuracy of 3.7 ± 0.4 pixels for the full trajectory model and 2.9 ± 0.4 pixels for the reduced trajectory model.

4. CONCLUSIONS AND FUTURE WORK

This paper has described a method for georeferencing MTI imagery based on photogrammetric principles. The PIR method was successfully used to georeference an MTI image. The absolute accuracy was on the order of 3 IR-sized pixels, while the band-to-band registration was subpixel in an average sense. Of particular note is the fact that similar geolocation accuracy was obtained from two different trajectories; a full trajectory model which did not match the actual motion of the MTI sensor, and a reduced trajectory model which more closely resembled the actual motion of the satellite.

The trajectory characteristics derived by the reduced trajectory model matched the measured exterior orientation parameters more closely. Also, the overall planimetric accuracy was higher for the imagery georeferenced through use of the reduced trajectory model than for the imagery georeferenced through use of the full trajectory model. Even though the reduced trajectory model did not include the pitch motion of the MTI satellite, accurately georeferenced imagery was still obtained. Therefore, given a choice between trajectory models, the more simple trajectory model (i.e. reduced) would be the preferred trajectory.

The disagreement between the exterior orientation parameters of the full trajectory model and the measured values is most likely due to coupling between the position and attitude parameters. For example, imagery collected through the motion of the sensor model in the X_{geo} direction can be duplicated by pitch motion, and similarly imagery collected through motion in the Y_{geo} direction can be duplicated by roll motion. Therefore, this coupling may be the cause of the inability of the photogrammetric bundle adjustment to calculate both the linear motion as well as the pitch motion of the sensor during image acquisition.

In closing, the particular MTI image used in this research is very close to a perfectly nadir acquisition (i.e. all three attitude angles are less than 2 degrees). Therefore, experiments with off-nadir imagery should be conducted to determine if the PIR method can accurately georeference LEVEL1B_U imagery containing larger misregistration effects.

ACKNOWLEDGEMENTS

We have benefitted from the support and advice of the entire MTI team. In particular, conversations with Bill Clodius concerning MTI image acquisition dynamics were especially useful. Enlightening conversations with Steve Bender, Bill Atkins, and Cindy Little concerning the layout of the focal plane and geometric calibration of the sensor optics are gratefully acknowledged. Also, conversations with our colleagues at Sandia National Laboratory in Albuquerque, NM, especially Tom Stueber, Max Decker, and Ron Kidner, were helpful in understanding the timing sequence and maneuvering of the MTI satellite. This research was supported by the U.S. Department of Energy.

DISCLAIMER

Mention of brandnames in this paper does not constitute an endorsement by the authors nor their employer.

REFERENCES

1. J. J. Szymanski, W. Atkins, L. Balick, C. C. Borel, W. B. Clodius, W. Christensen, A. B. Davis, J. C. Echohawk, A. Galbraith, K. Hirsch, J. B. Krone, C. Little, P. Maclachlan, A. Morrison, K. Pollock, P. Pope, C. Novak, K. Ramsey, E. Riddle, C. Rohde, D. Roussel-Dupré, B. W. Smith, K. Smith, K. Starkovich, J. Theiler, and P. G. Weber, "MTI Science, Data Products and Ground Data Processing Overview," *Proc. SPIE* **4381**, pp. 195-203, 2001.
2. P. Pope, J. Theiler, and A. Galbraith, "LANL Experience with Coregistration of MTI Imagery," to appear in *Proc. SPIE* **5159**, 2003.
3. J. Theiler, A. Galbraith, P. Pope, K. Ramsey, and J. Szymanski, "Automated Coregistration of MTI Spectral Bands," *Proc. SPIE* **4725**, pp. 314-327, 2002.
4. T. Henson, L. Krumel, D. Blake, D. Byrd, W. Christensen, W. Rappoport, and G. Shen, "Multispectral Thermal Imager Optical Assembly Performance and Integration of the Flight Focal Plane Assembly," *Proc. SPIE* **3753**, pp. 359-368, 1999.
5. W. B. Clodius, S. C. Bender, R. R. Kay, B. W. Smith, W. H. Atkins, W. Christensen, C. K. Little, E. F. Zalewski, and W. M. Rappoport, "MTI On-orbit Calibration," *Proc. SPIE* **3753**, pp. 380-391, 1999.
6. C. C. Slama, editor, *Manual of Photogrammetry*, Fourth Edition, American Society of Photogrammetry, Falls Church, Virginia, 1056 pp., 1980.
7. P. R. Wolf and B. A. Dewitt, *Elements of Photogrammetry with Applications in GIS*, Third Edition, McGraw-Hill Book Company, New York, New York, 608 pp., 2000.
8. E. M. Mikhail, J. S. Bethel, and J. C. McGlone, *Introduction to Modern Photogrammetry*, John Wiley and Sons, New York, New York, 479 pp., 2001.
9. Interactive Data Language (IDL), Research Systems Inc., Boulder, Colorado, <http://www.rsinc.com/idl/>, 2003.
10. M. R. Mostafa, "PE&RS Direct Georeferencing Column: An Introduction," *Photogrammetric Engineering and Remote Sensing*, Vol. 67, No. 10, pp. 1105-1109, 2001.
11. P. Pope, "Rapid Intersection of Line-of-Sight Rays with a Digital Elevation Model: A Nearest Neighbor Approach," to appear in *Proc. ASPRS/MAPPS "Terrain Data: Applications and Visualization"*, October 28-30, Charleston, South Carolina, 2003.
12. TNT Map and Image Processing System (TNT MIPS), MircoImages Inc., Lincoln, Nebraska, <http://www.microimages.com/products/tntmips.htm/>, 2003.
13. Environment for Visualizing Images (ENVI), Research Systems Inc., Boulder, Colorado, <http://www.rsinc.com/envi/>, 2003.